Cell

Domain Reorientation and Rotation of an Intracellular Assembly Regulate Conduction in Kir Potassium Channels

Oliver B. Clarke,[1,2] Alessandro T. Caputo,[1,2] Adam P. Hill,[3] Jamie I. Vandenberg,[3] Brian J. Smith,[1] and Jacqueline M. Gulbis[1,*]
[1]The Walter and Eliza Hall Institute of Medical Research, Parkville, Victoria 3052, Australia
[2]Department of Medical Biology, The University of Melbourne, Parkville, Victoria 3052, Australia
[3]Victor Chang Cardiac Research Institute, Darlinghurst, New South Wales 2010, Australia
*Correspondence: jgulbis@wehi.edu.au
DOI 10.1016/j.cell.2010.05.003

SUMMARY

Potassium channels embedded in cell membranes employ gates to regulate K^+ current. While a specific constriction in the permeation pathway has historically been implicated in gating, recent reports suggest that the signature ion selectivity filter located in the outer membrane leaflet may be equally important. Inwardly rectifying K^+ channels also control the directionality of flow, using intracellular polyamines to stem ion efflux by a valve-like action. This study presents crystallographic evidence of interdependent gates in the conduction pathway and reveals the mechanism of polyamine block. Reorientation of the intracellular domains, concomitant with activation, instigates polyamine release from intracellular binding sites to block the permeation pathway. Conformational adjustments of the slide helices, achieved by rotation of the cytoplasmic assembly relative to the pore, are directly correlated to the ion configuration in the selectivity filter. Ion redistribution occurs irrespective of the constriction, suggesting a more expansive role of the selectivity filter in gating than previously appreciated.

INTRODUCTION

Potassium currents across cell membranes are essential for the propagation of electrical signals in multicellular organisms, notably in the recovery phase of action potentials. Conduction occurs via the highly selective pore of K^+ channels and is switched on and off in response to regulatory cues. The switching process utilizes specific regions of the ion permeation pathway, termed gates, which are thought to work by altering the diameter of the pore or otherwise modifying the energetic barrier to permeation. Ion conduction is contingent upon gates in the permeation pathway adopting an open status. A weakness of present paradigms describing the nature of the gates and gating process is that they are predicated upon comparison of unrelated K^+ channel structures.

Potassium channels are tetramers, with the ion conduction pathway forming at a common subunit interface coincident with the molecular axis. Within its conserved core, each subunit comprises two transmembrane helices (inner and outer) supporting a shorter angled pore-helix spanning the outer leaflet of the membrane (see Figure 1A for nomenclature). This molecular scaffold serves to position a flexible ion selectivity filter. Considerable functional evidence based on pore-blocking and binding studies suggests that a gate is located at the inner-helix bundle at the face of the membrane (Armstrong, 1969, 1971; Armstrong and Hille, 1972; Baukrowitz and Yellen, 1996; Miller, 1987; Yellen et al., 1991), and it is thought to govern K^+ access by adopting discrete closed or open conformations. Substantial conformational variation in reported structures lends qualified support to this hypothesis. While the inner helix conformation in structures of KcsA is invariant, elegant mutagenesis studies from the Perozo laboratory have demonstrated that alternative conformations are accessible. Additional evidence is provided by Zhou, who identified electron density representing the bulky organic tetrabutylantimony within the permeation pathway of C-terminally truncated KcsA (Yohannan et al., 2007). Nonetheless, a K^+ channel from chlorella virus (ATCV-1) gates despite the inner helices being too short to cross over (Gazzarrini et al., 2009), implying that the selectivity filter in ATCV-1 is acting as a classical activation gate. Analogously, evidence that large permeant ions enter freely past the bundle crossing of large-conductance BK channels in their closed state (Wilkens and Aldrich, 2006) implies that the selectivity filter may act as a primary gate in that family.

Since the discovery of C-type inactivation (Hoshi et al., 1991) in *Shaker* channels, several lines of evidence have implicated the ion selectivity filter in gating. Single-atom substitutions involving exchange of amide with ester carbonyls in the selectivity filter exhibit dramatic effects on gating kinetics and conductance (Lu et al., 2001). Pore helix mutants of KcsA that perturb interaction of Glu71 with the signature Asp (GYGD) alter inactivation kinetics while leaving gating at the helix bundle crossing unaltered (Cordero-Morales et al., 2006; Cordero-Morales et al., 2007). Fluorescence lifetime measurements carried out on wild-type and pore helix mutants of KcsA labeled

at the bundle crossing reveal comparable bimodal distributions, which are inconsistent with the open probability assessed by single-channel recordings (Blunck et al., 2006), suggesting that other factors influence ion permeation. There is also evidence that gating at the intracellular bundle crossing is coupled to gating at the selectivity filter (Ader et al., 2009; Baukrowitz and Yellen, 1995) (Gao et al., 2005). For pore gating to be effectively studied, both the bundle crossing and the selectivity filter must be considered, and whether and how they communicate with one another ascertained.

Inward rectifiers (Kir) are ligand-gated K^+ channels that stabilize the resting membrane potential (Hille, 1992, and are important in cardiac (Gribble et al., 1998) and pancreatic function (Ashcroft et al., 1988). Their defining characteristic is that ion efflux is naturally stemmed by diffusion of cellular factors into the conduction pathway, occluding intracellular ion access. Physiological blockers include polyvalent cations such as putrescine, spermidine, and spermine (Lopatin et al., 1994) and, to a lesser extent, the divalent cations Mg^{2+} and Ca^{2+} (Matsuda et al., 1987; Vandenberg, 1987). Kinetic studies indicate that polyamine block is a sequential process, where intracellular binding sites harbor rectification agents prior to deep block in the transmembrane pore (Shin et al., 2005).

The study described here uses Kir channels to investigate molecular reorganisation during K^+ channel gating. Comparative analysis of a series of prokaryotic Kir channel structures reveals that the ion distribution in the selectivity filter is systematically correlated to conformational changes elsewhere in the assembly and that transmission of signals to the pore involves the intracellular N and C termini of the channel acting on the intracellular domains. Changes in selectivity filter configuration occur without widening at the helix-bundle crossing, suggesting a more prominent role for the selectivity filter in gating than has previously been appreciated. Moreover, identification of the polyamine binding sites in occupied and unoccupied states lends valuable clues to mechanism and indicates that polyamine release from an intracellular site to the permeation pathway is synchronous with specific conformational changes in the intracellular assembly heralding activation.

RESULTS

Structure Determination

We took advantage of substantial recent improvements in data correction and refinement algorithms (Adams et al., 2002; Strong et al., 2006) to reinterrogate improved density maps of three structures determined previously. The structures of KirBac1.1 (1P7B) and KirBac3.1 (1XL4 and 1XL6) were refined with data deposited in the PDB. New refinement statistics for these structures (I, II, and VIII, respectively) are included in Table S1 (available online). In structure I (3.7 Å), more of the N terminus was traceable than previously, and eight peaks of strong positive difference density at the junction of inner, outer, and slide helices were modeled as partial phospholipids carried through in the purification. After evaluation of the possibilities, an outer site (10.5 σ in omit maps) was assigned as the tertiary amine moiety of a neutral phosphatidyl choline, but equally may represent the head of an anionic lipid. The inner site (12.5 σ) was judged to accommodate a phosphate. While the hydrocarbon tails were insufficiently ordered for modeling, weak electron density consistent with their presence is located alongside aliphatic side chains of the inner and slide helices. New refinements of 1XL4 (II) and 1XL6 (VIII) took into account that both crystals had been soaked in 50 mM spermine prior to data collection (soaking solutions respectively contained $MgCl_2$ or $CaCl_2$). In both II (2.6 Å) and VIII (2.8 Å), spermine was modeled into contiguous residual electron density that was not present in the maps of any other structure (the highest peak in each instance is 8 σ). The R_{free} of VIII was significantly reduced by inclusion of a conformational variant at 40% occupancy.

Five new structures (III–VII) of KirBac3.1 were phased by molecular replacement, using previously determined KirBac3.1 structures (1XL4 and 1XL6) as search models. Full-length histidine-tagged recombinant channels crystallized in a range of space groups, diffracting to resolution limits between 3.1 and 4.2 Å. Crystallization conditions, data collection, reduction, and refinement statistics are provided in Tables S1 and S2.

In addition, three structures of a point mutant of KirBac3.1 (Q170A) were determined. The mutant channels are structurally and functionally similar to the wild-type, but consistently exhibit superior diffraction, and are used here for this reason (range 2.7 to 3.3 Å). Of crystals IX–XI derived from identical conditions, X was soaked in 5 mM $BaCl_2$ and XI in 2 mM samarium acetate (Sm^{3+} is isosteric with Ca^{2+}), and data were collected at wavelengths that maximized the anomalous signal. The only apparent peak (28 σ) in anomalous difference maps (15–5 Å) of X is consistent with Ba^{2+} binding in the selectivity filter. While the possibility of minor sites cannot be ruled out, none were obvious. Two strong peaks (18 and 11 σ) in the anomalous difference density of XI unequivocally identified Sm^{3+} binding sites at Asp36 and Glu173, respectively. In structure XI, electron density representing the outer transmembrane helices is stretched out, indicating high anisotropic mobility, which was verified by TLS modeling.

Twisting: Global Conformation Is Correlated to Slide Helix Orientation

Nomenclature is depicted in Figure 1A, and a reference summary of the structures is provided in Table 1. The three-helix topology describing the canonical pore of K^+ channels (Doyle et al., 1998) is elaborated by an amphipathic slide helix, first observed in the structure of KirBac1.1 (Kuo et al., 2003), and the N- and C-terminal domains of all four subunits coalesce into an intracellular assembly. No significant differences are discernable in the transmembrane regions of the channel; superposition of the Cα positions in the transmembrane helices of the 11 structures relative to structure VII yields an RMSD of <1 Å on 91 Cα atoms [residues 45–135 inclusive (Figure 1B and Figure S1A), with the exception that in KirBac1.1 (I) residues 92–96, corresponding to a distinctive turret conformation, were omitted]. The conformation is essentially as observed for Kir2.2 (Tao et al., 2009).

The structures cluster into two groups with distinct conformations, independent of space group and crystal form. The difference between the groups corresponds to a rigid body rotation of 23° (viewed from the membrane), about the molecular fourfold, of the entire intracellular assembly relative to the transmembrane pore (Figure 1C) (Movie S1). The global nontwist

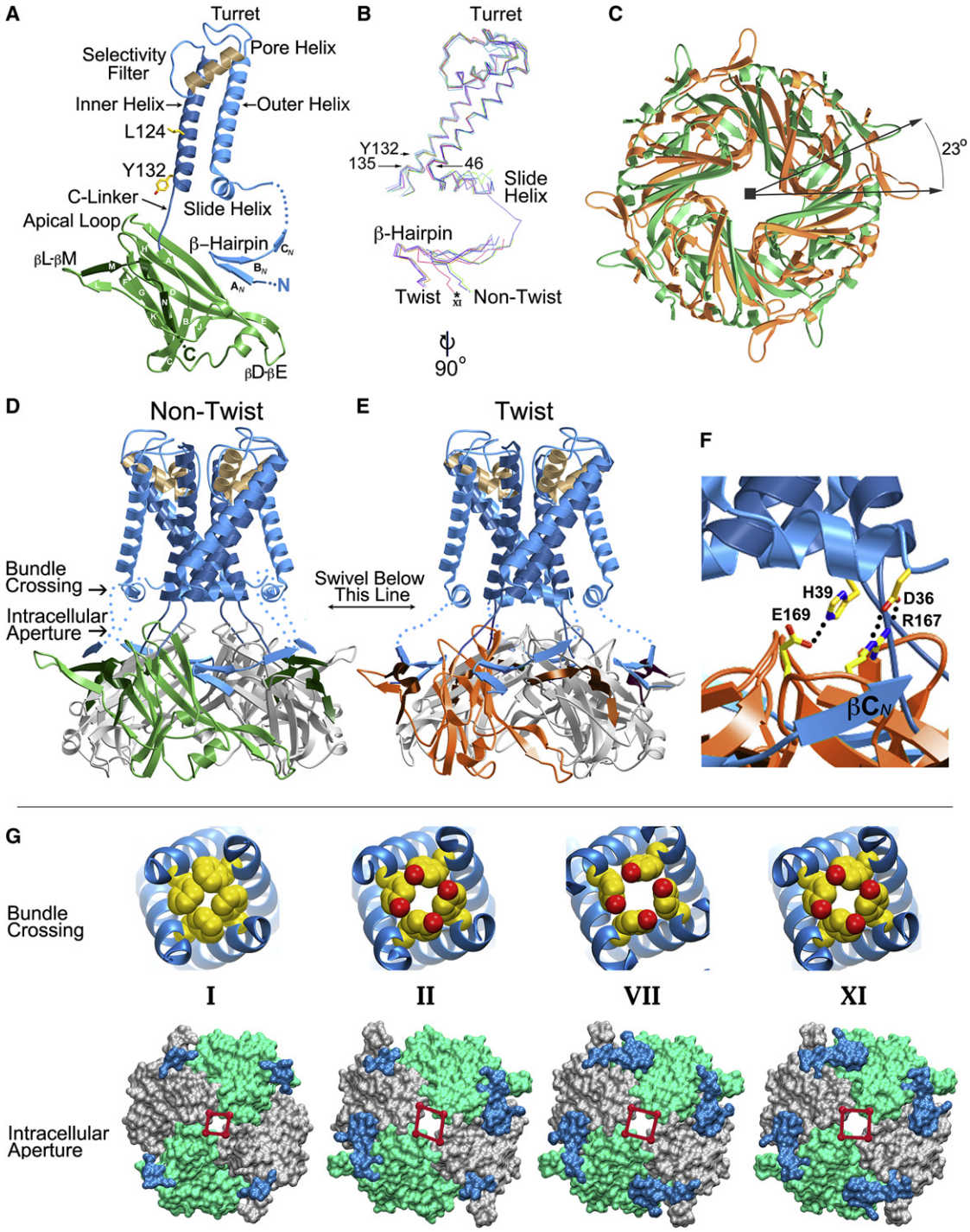

Figure 1. Two Conformations Are Related by a Rotation of the Intracellular Assembly Relative to the Pore

(A) Nomenclature. Y132 indicates the position of the bundle crossing.

(B) A single subunit of each of the 11 structures is superimposed over the transmembrane scaffold (residues 45 to 135) of structure VII. The structures diverge significantly only in the intracellular region, where conformational changes in the vicinity of the β hairpin and slide helices cluster according to twist. *XI (pink) represents a slide helix/β hairpin outlier due to destabilization of molecular contacts by Sm^{3+}.

(C) The intracellular assemblies of a twist (orange) and nontwist (green) channel are viewed from the membrane relative to superimposed pore domains (not shown).

(D) Gating intermediate II viewed in the plane of the membrane. The N terminus and membrane region are sky blue, the pore helices tan, and the intracellular assembly gray, with one subunit picked out in green.

(E) In structures III–VII, the intracellular assembly (orange and gray) is rotated by 23° relative to structure II.

Table 1. Comparison of Differentiating Features in Structures I–XI

KirBac ID	Structure ID	Space Group	Molecular Symmetry	β Hairpins Present	Interfaces Latched[c]	Interfaces Unlatched[c]	Interfaces Q170A[c]	Intracellular Status	Interdomain Conformer	Other Ions in SF	Ion Sites Occupied	Selectivity Filter Status
1.1	I	*I*222	four-fold	0	4	0	–	Latched	Nontwist	Mg^{2+} (Block)	S1, S2, S3/4 (S3/4 = Mg^{2+})	Blocked
3.1	II	$P2_12_12$	two-fold	2	2	2	–	Semi	Nontwist	Ca^{2+} (Block)	S1, S2, S4 (S4 = Ca^{2+})	Blocked
3.1	III	$P2_12_12$	two-fold	2	2	2	–	Semi	Twist	–	S1, S3, S4	Stalled
3.1	IV	*I*222	two-fold	2	2	2	–	Semi	Twist	–	S1, S3, S4	Stalled
3.1	V	$C222_1$	one-fold	3[a]	1[a]	2[a]	–	Semi	Twist	–	S1, S3, S4	Stalled
3.1	VI	*P*1	four-fold	4	0	4	–	Unlatched	Twist	–	S1, S3, S4	Stalled
3.1	VII	$P42_12$	four-fold	4	0	4	–	Unlatched	Twist	–	S1, S3, S4	Stalled
3.1	VIII	$P2_12_12$	four-fold	4	0	4	–	Unlatched	Nontwist (60%)[b]	–	S1, S2, S3, S4	Conductive
3.1 Q170A	IX	$P42_12$	four-fold	4	–	–	4	[d]	Twist	–	S1, S3, S4	Stalled
3.1 Q170A	X	$P42_12$	four-fold	4	–	–	4	[d]	Twist	Ba^{2+} (Block)	S1, S2, S4 (S4 = Ba^{2+})	Blocked
3.1 Q170A	XI	$P42_12$	four-fold	4	–	–	4	[d]	Nontwist	–	S1, S2, S3, S4	Conductive

Definitions are provided in the text. Note that "Selectivity Filter Status" (final column) represents an *interpretation* based on preceding columns of correlated parameters.

[a] In structure V, a crystal lattice contact results in more pronounced asymmetry of the intracellular domains.

[b] Both conformations are evident in the crystal lattice, but only the one corresponding to the major fraction is listed.

[c] See Figure 3 and Figure S6.

[d] The conformation at the subunit interface of Q170A is unique: close to unlatched but lacking some molecular interactions.

conformation of structure II (Figure 1D) is representative of structures I, II, and Q170A XI. In the remainder (native IV–VII; Q170A IX–X), the alternative twist conformation occurs (Figure 1E), and an accompanying rotation of the slide helices about an orthogonal axis brings the side chains of residues His39 and Asp36 into register with Glu169 and Arg167 (respectively) (Figure 1F and Figures S1B and S1C), stabilizing the conformation. In nontwist structures, there are no obvious interdomain stabilizing contacts. In crystals of VIII, where the nontwist conformer is present at 60% occupancy and the twist conformer at ~40%, both conformations of the slide helix are refined. The constriction at the helix bundle crossing is essentially identical in all structures, notwithstanding small differences in the position of a blocking side chain, whereas the aperture to the cytoplasmic assembly (18 Å below the bundle crossing) exhibits systematic variations of up to 6 Å (Figure 1G).

Interdomain Linkers Are Reconfigured by Bound Phospholipids

The C linkers are extensions of the inner helices that connect the pore to an intracellular C-terminal domain and have been implicated in the phosphatidyl inositide (PIP_2) sensitivity of eukaryotic Kirs (Huang et al., 1998; Lopes et al., 2002; Soom et al., 2001) and noted as a hotspot for PIP_2-sensitive residues (Logothetis et al., 2007). In structure I, which has an additional arginine in the C linker, specific interactions between phospholipid and conserved residues (Figures 2A and 2B and Figure S2) restrain the C linkers. An exclusive set of interactions, involving arginine and proline residues in the C linker (Figures 2C and 2D), compresses the intersubunit spacing at the vestibule entrance (Figures 1D and 1G), stabilizing a constriction and isolating an intracellular vestibule from the pore. Despite a three-residue insertion that alters the curvature of the C linker and adds additional charges (Tao et al., 2009), Kir2.2 exhibits very similar features to the structures without bound lipid.

Unlatching: Two Molecular Arrangements Characterize Subunit Interfaces

Eight wild-type structures pinpoint regions of the channel that alternate between distinct conformations, revealing correlated structural changes. Two discrete molecular arrangements at

(F) Two polar interactions linking the slide helices to the intracellular assembly stabilize the twist conformation. Figures were prepared with Molscript (Kraulis, 1991).

(G) Representative structures depicting the constriction at the helix bundle crossing (above) and intracellular aperture (below). The inner helices of I, II, VII and XI are depicted, with CPK representations of Tyr132 (Phe146 in I). The surface of the intracellular tetramer (residues 136–295) is viewed from the membrane, with red spheres representing the Cα of Gln252 (266 in I as a positional marker for the constriction). The red spheres are joined to indicate the constriction in I, diagonal distortion in II, and a wider aperture in VII and XI.

See also Figure S1 and Movie S1.

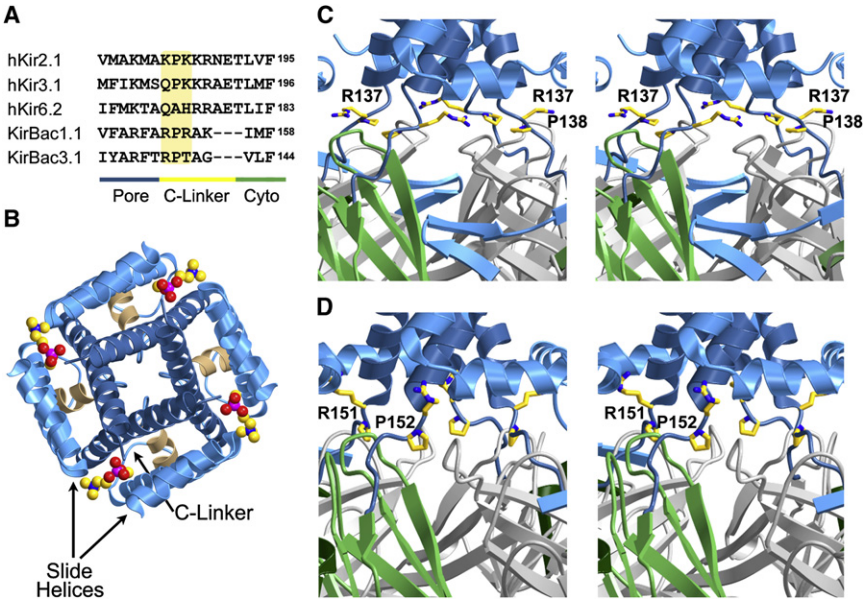

Figure 2. Structural Phospholipids Reconfigure Interdomain Linkers, Stabilizing a Narrow Aperture to an Intracellular Vestibule

(A) The critical residues (highlighted) are two polar residues separated by a small hydrophobic residue.

(B) The well-ordered head group of a structural lipid molecule (P, magenta spheres; O, red; C, yellow; N, blue) at the junction of inner, outer and slide helices connects adjacent subunits.

(C) Stereoview. In structures II–VIII, no ordered phospholipid is present, and the subunits are spaced apart at the apex. Arg137 stabilizes the spacing, making two hydrogen bonds to the βH-βI loop of the adjacent subunit.

(D) Stereoview. In structure I, Arg151 and Arg153 contact the slide helix and bound phospholipid (for clarity, phospholipid is not shown), and Pro152 packs against the βH-βI loop, confining the C linkers centrally.

See also Figure S2.

subunit boundaries (Figure 3A) accommodate different orientations of individual intracellular domains.

In structures II–IV, two arrangements (described hereafter as latched and unlatched) alternate about the four-fold (Figures 3B and 3C and Figures S3A and S3B). This reduces the symmetry of the assembly to two-fold, and, although not appreciable in the transmembrane pore, it is apparent in the intracellular domains (Table 1). The key features are a salt bridge between two highly conserved Kir residues (Figure S3C) and an N-terminal β hairpin (A_N-B_N) that spans unlatched subunit interfaces (Figure S3D) but is only partially ordered at latched interfaces (Table 1). Additionally, the loops βD-βE and βL-βM are only well ordered at unlatched interfaces.

Intersubunit connections are clustered near the membrane in the latched arrangement, but they reorganize, in the unlatched arrangement, into a more extensive array of interactions. The net effect of staged unlatching at all four interfaces (structures VI–VIII) is a symmetrical iris-like dilation of a narrow opening to the intracellular vestibule by approximately 4.5 Å relative to I (Figure 1G), extending the permeation pore through both domains (Movie S2). The opening in question is located 18 Å from the bundle crossing (Figure 1D).

Molecular Pulleys Link Unlatching to Domain Reorientation

Structural interdependency links rearrangement at the subunit interfaces to systematic reorientation of the intracellular domains, where latched and unlatched differ by approximately 5°. Coupling is facilitated by actions of the N and C termini, which effectively act as a pulley system. The intracellular domain of each subunit is an immunoglobulin-like β sandwich, overlaid on the surface by N and C termini. Its C terminus is tethered both to the N terminus and the underlying β sandwich such that all motions are interdependent. In addition, parallel β sheet interactions formed between βC_N on one subunit and βM on another (Figure 3D) adapt the basic fold by interweaving neighboring subunits into a circle, coupling the motion of each subunit to that of its neighbor.

Twin Polyamine-Binding Sites Are Identified

Distinct polyamine-binding sites have been identified in the intracellular assembly and pore, and in the presence and absence of bound polyamines.

In II, spermine molecules partially buried within the two latched subunit interfaces are modeled in alternate conformations distinguished by their interactions with neighboring residues (Figure S4A). Two counter ions designated as chlorides are coordinated by side chains at the interface. The intracellular pockets are preformed, those in II superimposing closely with the latched interface in the corresponding unliganded structure III.

The open-ended sites accommodate polyamines of variable length oriented parallel to the molecular axis. In II, one end of each spermine points toward the pore (Figure 4A), while the other juts from a distal opening such that the amines farthest from the membrane are exposed and hydrated. A trio of residues, His177 and Asp197 from one subunit and Arg204 from another, enclose the aliphatic pocket, while another (His255, Glu173, Thr 244) lies between the polyamine and the bundle crossing (Figure 4B). The morphology of each binding pocket is determined by domain orientation; at unlatched interfaces the pockets are diminished and incompatible with polyamine binding (Figures 4C and 4D). In XI, Glu173 coordinates Sm^{3+}, suggesting that the intracellular binding pocket is a general cation-binding site (Figure S4B).

In VIII, an axial spermine occupies the permeation pathway, entering as far as the symmetry-related side chains of Leu124 (Figures 4E and 4F and Figure S4C). In the other KirBac structures, as well as some structures of KcsA (e.g., Phe103 in PDB 2IH3), an equivalently sited residue similarly constricts the permeation pathway. In the Kir family, a moderately sized residue is conserved at this position, where an acidic side chain characterizes strong inward rectifiers (Wible et al., 1994). In

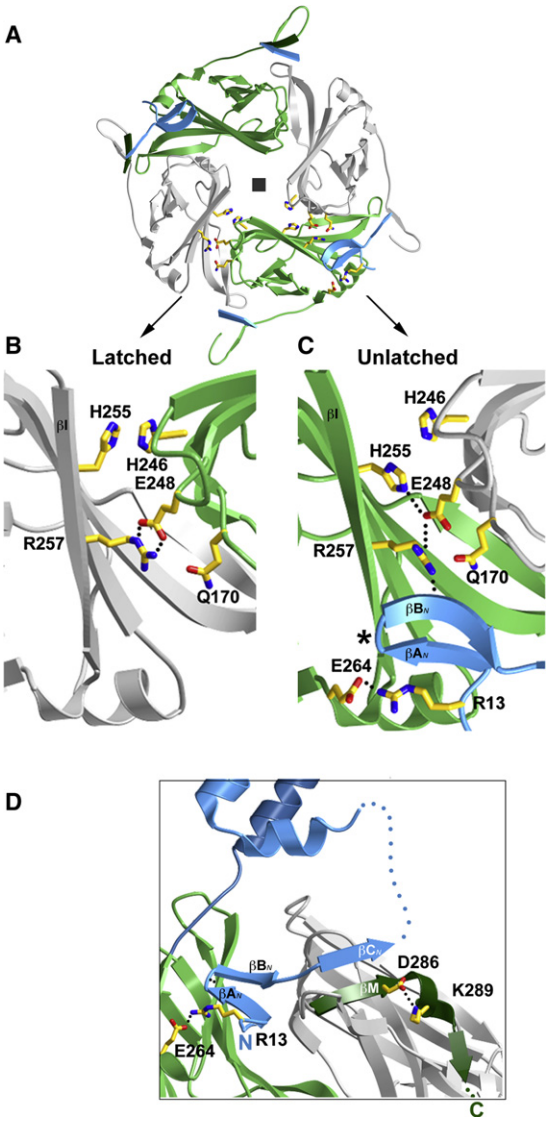

Figure 3. Two Distinct Molecular Arrangements Characterize Subunit Interfaces

(A) The symmetry of the intracellular assembly of II, viewed from the membrane along the molecular axis, is pseudo-four-fold. Adjacent subunits are colored green and gray.

(B) Close-up view of the latched intracellular interface arrangement.

(C) The unlatched interface differs in that ordering of the βA_N-βB_N hairpin relocates the core interactions further from the membrane (the * denotes a backbone amide interaction connecting an amide oxygen at the reflex point of the hairpin to an amide nitrogen on βI located across the interface).

(D) Molecular pulleys determine subunit orientation: parallel β sheet interactions formed between βC_N on one subunit and βM (dark green) on another interweave neighboring subunits. A turn of amphipathic helix connecting βM to βN firmly anchors βM to the underlying scaffold (gray and mid-green). The β hairpin (A_N-B_N) is connected back to its originating subunit by a β sheet interaction with βI (a single hydrogen bond at the inflection of the β-hairpin). A salt bridge, R13…E264, positions the N terminus.

See also Figure S3 and Movie S2.

Kir2.1, for example, the Leu124 equivalent is Asp172, and point mutations decrease the binding affinity of polyamines (Guo et al., 2003). Held in place by extensive van der Waals contacts, the extended spermine molecule protrudes out of the membrane, forming a cation-π interaction between the aromatic ring of Tyr132 at the bundle crossing and the secondary amine, indicating that as for the intracellular binding site a range of polyamine lengths can be accommodated.

Ion Configuration Is Linked to the Global Conformation of the Channel

A major finding is that the number and site distribution of bound ions in the selectivity filter are contingent on global conformational changes. Although the moderate resolution of the structures (2.6 to 4.2 Å) does not differentiate changes in the backbone conformation of the flexible selectivity filter, the positions of bound ions are clearly discernable (Figure 5A). For convenience, discrete ion binding sites are denoted S1 to S4 (Figure 5B) after Roux (Bernèche and Roux, 2001). The Q170A structures are included in the analysis, as the pore does not differ from wild-type protein.

To briefly summarize, the twist structures are characterized by a specific three-ion configuration (S1, S3, S4). In nontwist forms, four sites are occupied (S1, S2, S3, S4), corresponding to a weighted mean of contributing two-ion and three-ion configurations averaged over the crystal. When divalent ions occupy the selectivity filter, a cation-specific blocked configuration occurs (S1, S2, S4 = M^{2+}). The details are elaborated below.

Structure I has three occupied ion sites: S1, S2, and an innermost site located between the previously described S3 and S4 locations, where it is coordinated by the carbonyls of Thr110. We suggest that the S3/S4 site ion represents Mg^{2+}, rather than a K^+ as initially reported (Kuo et al., 2003). Mg^{2+} was present in crystallization conditions and ion coordination distances persistently refine to approximately 2.1 Å, inconsistent with K^+ or water. The density is consistent with either square planar or pentacoordinate geometry (with an axial water), both inappropriate to K^+ coordination. The S3/S4 site corresponds to a putative Li^+ binding site inferred on the basis of a combined electrophysiology, molecular dynamics, and crystallographic analysis (Thompson et al., 2009) and is most likely to represent a Mg^{2+}-blocked configuration.

Similarly, in II, which has two-fold symmetry, only three sites S1, S2, and S4 are occupied. The ion distribution is exclusive to this structure, and interatomic distances of 2.4–2.5 Å between carbonyl oxygens and the ion are indicative that S4 coordinates a Ca^{2+} ion (present in crystallization conditions).

In the twist structures III–VII and IX, the ion configuration is S1, S3, and S4. This distribution concurs with a predicted three-ion conduction substate, *d* (in the notation of Bernéche and Roux), in the low free energy pathway (Bernèche and Roux, 2001), and potentially represents a direct view of substate *d*. Shifting between multiple substates is a prerequisite for conduction, however, implying that a single stable substate configuration equates to stalled or inactive conduction status. In X, despite the twist, a Ba^{2+} bound at S4 stabilizes the filter in a blocked configuration (S1, S2, S4) similarly to I and II (Figure S5A).

Two structures, VIII (60% nontwist, 40% twist) and XI (100% nontwist), have all four sites occupied. This indicates

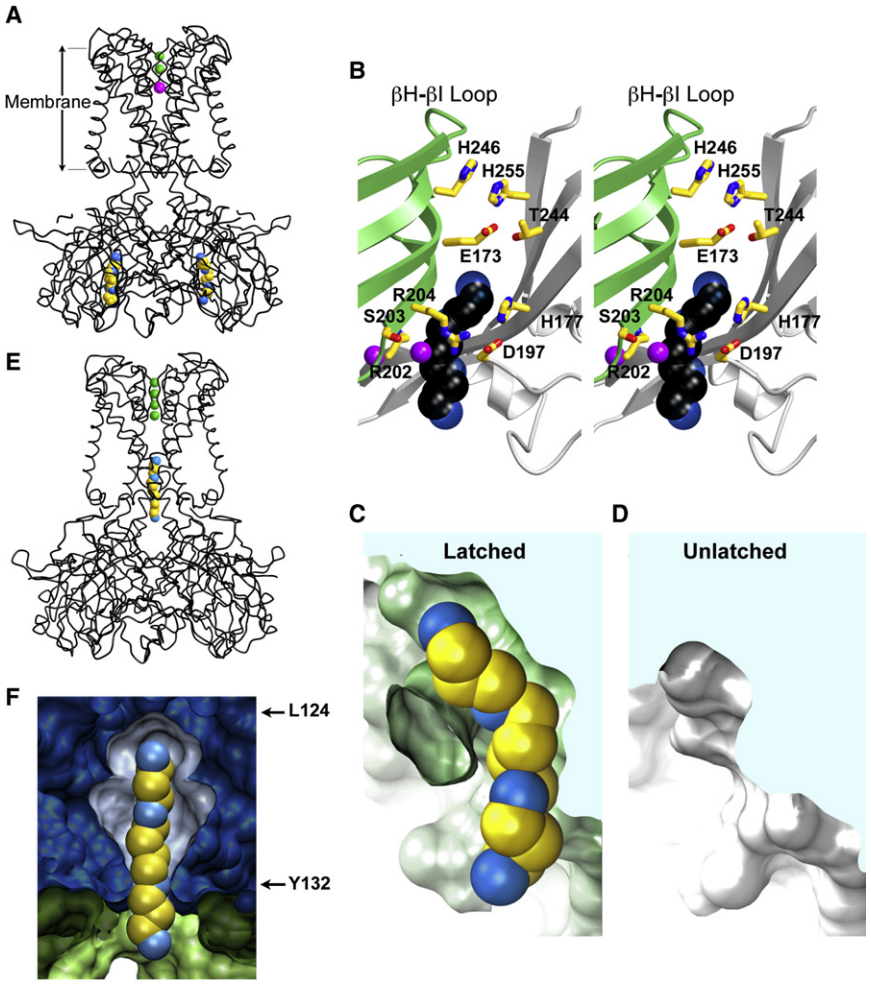

Figure 4. Identification of Two Polyamine-Binding Pockets

(A) The latched intracellular interfaces accommodate polyamines within a closed pocket. The Cα trace of II is represented as a black coil, with two symmetry-related spermine molecules represented by colored spheres (N atoms are cyan; C atoms are yellow).

(B) Stereoview of the intracellular binding pocket observed from *within* the vestibule, with interacting side chains depicted as sticks. The stacked histidine side hains are just beneath the membrane (see Figure 3). Spermine is represented by CPK spheres with C atoms colored black (to contrast with the atoms from yellow side chains) and N atoms blue. Counter ons are depicted as violet spheres.

(C) A cutaway of the internal molecular surface of II shows that spermine fits easily into a binding pocket at a latched interface.

(D) A comparable view of the unlatched interface of II reveals morphology incompatible with polyamine binding (changes in position and side chain orientation of key residues backing the binding site, notably Pro206, Ile172, and Leu242, reduce the length of the pocket).

(E) Coil representation of the Cα trace of structure VIII, with axial spermine represented as CPK spheres.

(F) A longitudinal slice through the molecular surface of VIII the polyamine-binding site.

See also Figure S4.

a conducting, or open, conformation of the selectivity filter, consistent with predictions that the motions of ions in the filter during conduction are highly correlated and that the pathway of lowest free energy is via four contributing substates (Bernèche and Roux, 2001). We cannot rule out the possibility that the pattern of occupancy in VIII is an average of nonconductive twist (present at 40%: S1, S3, S4) and Mg^{2+} block (S1, S2, S3 = Mg^{2+}) configurations. There is, however, no evidence for Mg^{2+} at the position between S3 and S4 arguing, on balance, that VIII is in a conducting conformation and that Mg^{2+} block is not favored in the presence of spermine. Furthermore, the ion distribution in VIII, which binds an extended axial spermine in the permeation pathway, is indistinguishable from that of XI, which does not. Soaking crystal XI with a trivalent cation that shares some of the qualities of Ca^{2+} was particularly helpful, allowing us to capture the nontwist form of the channel without a blocked ion configuration (i.e. Sm^{3+} coordinates Asp36 on the slide helices, abrogating interactions with the C-terminal domains that stabilize the twist conformation) (Figure S5B). Structure XI is unique in exhibiting marked anisotropic mobility of the outer transmembrane helices (Figures S5C and S5D), suggesting that a lack of slide helix constraints and pore blockers permits increased thermal motion. The data are summarized in Figure 5C.

Recombinant KirBac3.1 Exhibits Subconductance States

Patch clamping carried out on purified wild-type KirBac3.1 channels reconstituted into giant unilamellar vesicles (GUVs) (Battle et al., 2009) showed functional ion channels with a predominant single channel conductance of 63 pS for both WT (Figure 6A) and Q170A (Figure 6B) mutant channels. The Q170A mutant (Figure S6) has a higher open probability than the wild-type channels. KirBac3.1 current recordings closely resemble reported recordings on KirBac1.1 (Cheng et al., 2009), including gating heterogeneity and a range of subconductance states (Figure 6C).

DISCUSSION

Evidence for selectivity filter gating derives from several sources (Baukrowitz and Yellen, 1995; Blunck et al., 2006; Cordero-Morales et al., 2006; Cordero-Morales et al., 2007; Hoshi et al., 1991). This study takes an important step, in which determination and analysis of multiple structures pinpoints areas of the molecular scaffold that undergo localized transition, globally correlates these changes, and lays a rational foundation for distinguishing structures of conducting K^+ channels from those that are nonconductive or blocked. Our findings provide strong evidence that the selectivity filter can switch between nonconducting and conducting configurations without significant displacement of the inner helices. This is distinct from findings

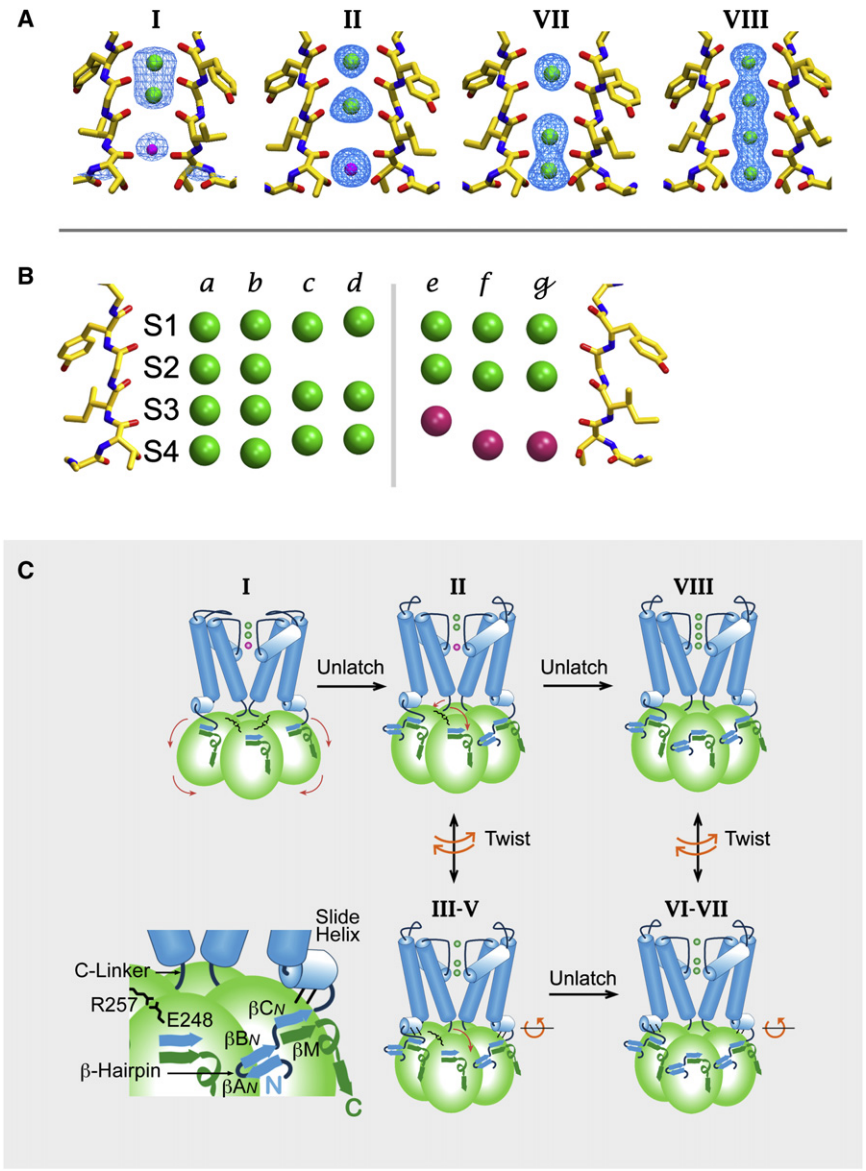

Figure 5. Ion Configuration Is Linked to Global Conformational Change

(A) Omit map $|Fo| - |Fc|$ contoured at 5 σ. K^+ ions are green, and $Mg^{2+}/Ca^{2+}/Ba^{2+}$ magenta (An $(2|F_o| - |F_c|)$ map at 4 σ is used for structure I.

(B) Refined ion sites positioned relative to the selectivity filter backbone of structure VIII indicate that K^+ channels have distinct conducting, nonconducting, and blocked configurations: a, VIII (conducting); b, 1K4C KcsA (conducting); c, VII (twist); d, 1K4D KcsA; e, I (Mg^{2+} block); f, II (Ca^{2+} block); and g, (Ba^{2+} block).

(C) Correlated structural changes shift the equilibrium status ion configuration. Roman numerals refer to the structures. The inset at lower left defines the structural elements. Top left: a nonconductive channel has four latched interfaces and a blocked selectivity filter. Top center: intermediate with alternating latched and unlatched interfaces; structure II (Ca^{2+} blocked) is depicted. Top right: four unlatched arrangements at subunit interfaces and a conductive selectivity filter. Bottom: the selectivity filter of all nonblocked twist conformers assumes a three-ion substate.

See also Figure S5.

that inactivation at the selectivity filter is driven by widening at the bundle crossing, and vice versa (Blunck et al., 2006; Cordero-Morales et al., 2007). While research into selectivity filter gating has primarily focused on C-type inactivation, our data indicate that the selectivity filter is not limited to this and is susceptible to subtle global conformational change, suggesting a more universal role in gating than hitherto expected. The correlation of twist to ion configuration in Kir channels suggests that global motions shift the equilibrium between conducting and nonconducting metastable states and is likely to be reversible on a short time scale. That the effect is mediated by the slide helices poses a plausible rationale for why disrupting interactions between slide helices and the intracellular domains of Kir2.1 leads to defective gating (Decher et al., 2007). It also supports an argument for generality of selectivity filter gating, as, unlike the intracellular assembly, the slide helices are conserved in most K^+ channels (e.g., the S4-S5 linker in Kv families). Importantly, our data indicate that ion distribution transcends channel type and reflects gating status. For example, the ion distribution observed in nontwist-nonblocked structures (VIII, XI) is identical, within coordinate error, to that in a 2.0 Å structure of conductive KcsA (Zhou et al., 2001), yet the occupancy in twist-nonblocked structures is comparable to that observed in a conduction-compromised state crystallized in an almost complete absence of K^+ (although S3 was assigned as water) (Zhou et al., 2001).

The KirBac structures collectively define a process of conformational interchange mediated at the intracellular subunit interfaces. The structures do not follow a conformational continuum, but rather illustrate a staged path to activation via two-fold symmetric intermediates, where in the midrange only every other subunit is unlatched, distorting the symmetry along a cross-sectional diagonal (Figure 1G and Table 1). Similar symmetry was observed for the ligand binding domains of a glutamate receptor (Armstrong et al., 2006; Sobolevsky et al., 2009), whereas in the K2P channels true bilateral symmetry becomes pseudo-four-fold at the selectivity filter (Kollewe et al., 2009), suggesting a common theme.

The combination of structure and function data indicates that unlatching, and consequent reorientation of the cytoplasmic domains, is coupled to the selectivity filter and hence represents an auxiliary gate in Kir channels. Our analysis shows that only when all four interfaces have eschewed the latched arrangement

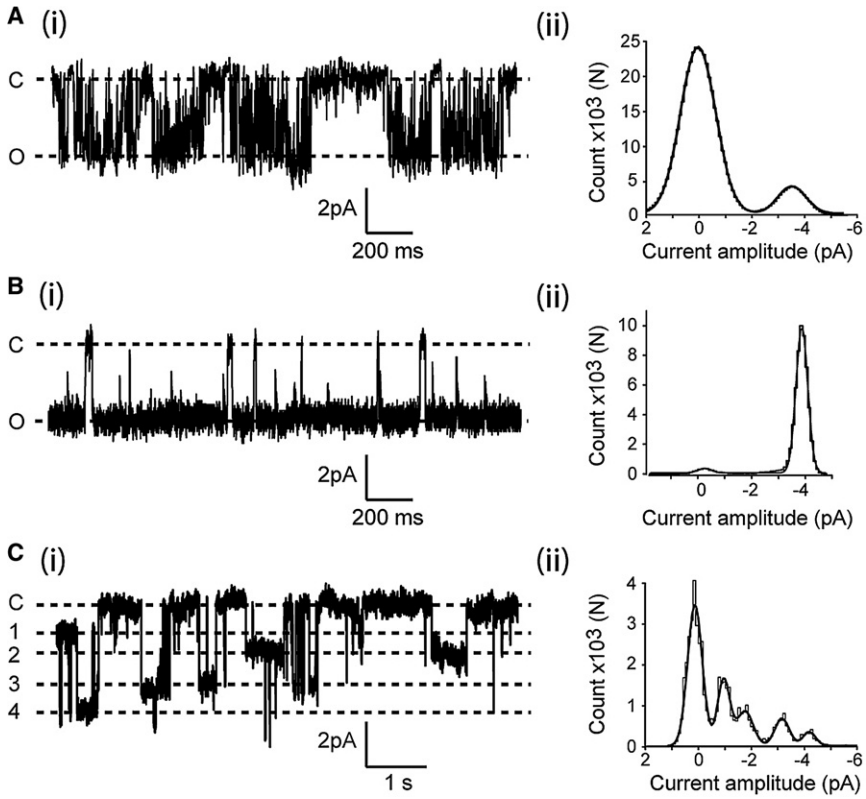

Figure 6. Purified Recombinant KirBac 3.1 Forms Functional Ion Channels in GUVs

(A and B) Single-channel recordings from wild-type (A) and Q170A mutant (B) KirBac3.1 channels.

(Ai and Bi) Individual channel traces recorded at a holding potential of −60 mV. Closed and open channel levels are labeled C and O, respectively.

(Aii and Bii) Representative all points amplitude histograms of KirBac3.1 channel activity from 100 s of continuous recording at −60 mV for the wild-type channel and 20 s of continuous recording for Q170A. Fits of Gaussian distributions to multiple histograms yielded at a single channel current of 3.7 ± 0.1 pA at −60 mV for both WT and Q170A channels.

(C) KirBac3.1 channels exhibit significant gating heterogeneity and subconductance states.

(Ci) Recording shown from a patch containing KirBac3.1 channels with multiple conductance states (dashed lines).

(Cii) All points amplitude histogram of the data shown in (Ci). Fits of multiple Gaussian distributions to the data showed peaks at 0, 1.15 pA, 2.01 pS, 3.49 pA, and 4.57 pA corresponding to the conductance levels in (Ci).

See also Figure S6.

can the selectivity filter acquire a conducting conformation, suggesting that unlatching is concomitant with activation. We note that the three Q170A mutants are effectively unlatched at all four interfaces but have fewer molecular constraints than the wild-type (Figure S6), resulting in a small, consistent, difference (~1°–2°) in the orientation of the cytoplasmic domains while the pore is unchanged. The structural difference is reflected in the higher open-probability of Q170A relative to the wild-type. Furthermore, fluorescence resonance energy transfer experiments on a series of differentially labeled Kir3.1/Kir3.4 heteromers indicate that activation entails a composite relative motion of the intracellular subunits, qualitatively consistent with unlatching (Riven et al., 2003).

The conformational interrelationships described herein suggest a general explanation for the effects of ligands and regulatory binding partners, such as the Gβγ subunits on Kir3 channels. We earlier described how the mutual orientation of adjacent intracellular domains is affected by the N and C termini of the protein. Perturbation of either terminus by a regulatory molecule is likely to elicit domain reorientation, presenting a means of rapid signal transmission from the intracellular assembly to the gates. By the same token, molecules preventing reorientation must stabilize the closed state. While Gβγ subunits are thought to utilize the N and C termini of Kir3 channels during activation (Jones et al., 2001), the binding site of ATP, which inhibits activation of Kir6 channels, has been attributed primarily to the N terminus (Tucker et al., 1998). Our hypothesis explains why functional experiments alone have been unable to pinpoint regulatory binding sites (e.g., PIP_2 and ATP) with any precision, as ligand binding at any point in the network could potentially draw an effect.

Kir channels also regulate current directionality, and this study illuminates specific features tailored to effect rectification. At resting potential, intracellular binding sites at latched interfaces locally concentrate cations. Unlatching causes the intracellular vestibule to connect with the pore, simultaneously disrupting the binding sites and facilitating polyamine release into an opening conduction path. A recent study of the isolated intracellular assembly of Kir3.1 correlates spermine binding to small changes at the subunit interface, leading the authors to conclude that polyamine binding stabilizes the resting state (Osawa et al., 2009). Although our structures indicate that the binding pocket is preformed, the essence of the argument, that binding is contingent upon the relative orientation of the subunits, is thermodynamically commensurate with our findings.

The geography of the intracellular polyamine-binding site provides a plausible explanation for experimental data implicating His216 in pH titratable rectification in Kir6.2 (Baukrowitz et al., 1999). In KirBac3.1, the counterpart of His216 is His177, which interacts with Asp197 in enclosing the binding pocket. Consistent with the Kir6.2 study, protonation of His177 at low pH would offset the negative charge of Asp197, reducing the electrostatic attraction of the site to polyamines, whereas at higher pH an unshielded negative charge would favor polyamine binding. In Kir channels, one or both of the residues corresponding to Glu173 and Thr244 is invariably acidic, maintaining a ring of negative electrostatic surface charge near the apex of the vestibule and favoring polyamine retention. In human Kir2.1, the

corresponding residues Glu224 (Taglialatela et al., 1995; Yang et al., 1995) and Glu299 (Kubo and Murata, 2001) have been implicated in rectification.

Spermine fully occludes the narrow pore entrance of VIII, consistent with findings that linear cations confer stronger rectification than bulkier molecules (Lopatin et al., 1994; Loussouarn et al., 2005), which may be unable to enter past the constriction. If opening a long pore is concomitant with polyamine release, entry of hydrated of K^+ ions ahead of the polyamine should be largely excluded. Further investigation will be essential to pin down the mechanistic aspects of current rectification and to provide an explanation for a small current efflux under depolarisation conditions (Guo et al., 2003; Lopatin et al., 1994).

The inner helix conformation determines the width at the bundle crossing and is commonly attributed to gating state. This has been questioned with reference to HERG (Hardman et al., 2007) and Kir channels (Shang and Tucker, 2008). To date, multiple structures of any native channel have exhibited identical conformations, suggesting that inner helix conformation may relate to the specific electrical signature of a channel or channel family rather than to its conduction status. For example, all crystal structures of K_v channels feature similar pronounced curvature of the inner helices. While perturbation at the bundle crossing unquestionably influences the open probability of channels, the way in which this is achieved is shaping up to be more complex than previously thought and provides ample fodder for discussion. It is notable that the only structure representing the large-conductance BK family has curved helices and a wide pore (Jiang et al., 2002), consistent with rapid ion and water diffusion. Aldrich's finding that a benzoyl-derivatised butyl quaternary ammonium does not become trapped in a closed BK channel (Wilkens and Aldrich, 2006) is consistent with a wide aperture at the bundle crossing in both open and closed states. It reinforces the argument that the selectivity filter can act independently as a permeation switch as well as a means of inactivation.

The study presented here provides evidence of selectivity filter gating distinct from C-type inactivation and governed by global conformational changes. As the relative twist determines the equilibrium status of the selectivity filter, it will be important to discern whether this is a threshold effect or a continuum. A continuum of tiny conformational adjustments of the selectivity filter transitioning between twist and nontwist forms could represent an ancillary influence in conduction, but whether such filter breathing contributes to the subconductance levels observed for KirBac channels remains to be established. Overall, we anticipate that the findings and analyses presented here will provide the groundwork for future investigations into K^+ channel action.

EXPERIMENTAL PROCEDURES

Protein Expression, Purification, and Crystallization

Full-length KirBac3.1 from *Magnetospirillum magnetotactium* and a Q170A mutant channel were expressed at 25°C in *E. coli* BL21 (DE3) star cells. After harvesting, cells were lysed at 20,000 psi in a high-pressure homogenizer. Protein was extracted by incubating the lysate with 1% Anzergent 3,12 at room temperature for 1 hr. Cellular debris was removed by centrifugation, and the protein was purified by affinity chromatography with Ni^{2+}-loaded IMAC resin, followed by size-exclusion chromatography. Peak fractions were pooled and concentrated to ~8 mg/ml for crystallization, which was carried out by vapor diffusion at 19°C at the Bio21 C3 crystallization facility. Precipitant conditions are listed in Table S2.

Data Collection and Processing

Data collection was carried out on cryocooled single crystals of KirBac3.1 at either the Australian Synchrotron (beamline 3BM1) or at the Swiss Light Source (microfocus beamline X06SA). New refinements of previously determined structures I, II, and VIII utilized publicly available data sourced from the Protein Data Bank under respective PDB codes 1P7B, 1XL4, and 1XL6. Data from 1P7B were anisotropically corrected with the National Institutes of Health (NIH) server at the NIH-MBI laboratory at University of California, Los Angeles (Strong et al., 2006). Test sets containing 5% of the reflections selected randomly or in thin resolution shells were flagged for noninclusion in refinement procedures.

Structure Determination and Refinement

Electron density in structures III–VII was phased by molecular replacement. Whole or partial models were derived from 1XL4 and 1XL6, with all ions and water molecules removed from the models prior to performing searches. Solvent flattening and histogram matching protocols were used to improve the electron density maps. Maps for structure I were B factor sharpened. Model building and refinement involved iterative refinement of atomic coordinates using maximum likelihood and simulated annealing procedures, alternating with cycles of TLS and individual or group B factor refinement. Refinement was monitored according to the decrease in R_{free}. A number of residues in each structure were omitted or had side chains truncated at Cβ due to positional disorder, and are listed in the PDB depositions.

Ion Channel Reconstitution

KirBac3.1 was incorporated into GUVs prepared by rehydrating lipids in sucrose solutions followed by protein reconstitution. In brief, a 10 mg/ml solution of 70:30 PE/PC lipid (Avanti Polar Lipids, AL) in chloroform was dried under N_2. Once dry, 3 μl purified water was added to the bottom (prehydration) followed by 1 ml 0.4 M sucrose. The solution was incubated for 3 hr at 60°C. Purified protein solubilized in 0.005% TDM was added at a 1: 200 protein-to-lipid ratio, and the solution was shaken on an orbital mixer overnight until a cloud of liposomes was seen to float in the solution. The sample was then shaken for a further 3 hr at room temperature in the presence of Bio-Beads (Bio-Rad) to remove traces of detergent.

Electrophysiology

An aliquot of liposomes (2–4 μl) was taken from the liposome cloud and introduced to the recording bath. Channel activity was examined in inside-out liposome patches with symmetrical bath and pipette solutions. Borosilicate glass pipettes were of a diameter that corresponded to a pipette resistance in the range of 3.0–5.0 MΩ. Ionic currents were recorded with an Axon 200B patch-clamp amplifier, filtered at 2 kHz, and digitized at 10 kHz. Single-channel analysis was done with pCLAMP10 software (Axon Instruments).

Complete experimental methods, including recipes for solutions and growth parameters, along with references, are provided in the Extended Experimental Procedures.

ACCESSION NUMBERS

Coordinates and structure factors have been deposited in the Protein Data Bank. Accession codes are as follows: I, 2WLL; II, 2WLJ; III, 2WLI; IV, 2WLO; V, 2WLM; VI, 2WLN; VII, 2WLH; VIII, 2WLK; IX, 2X6A; X, 2X6B; and XI, 2X6C.

SUPPLEMENTAL INFORMATION

Supplemental Information includes Extended Experimental Procedures, six figures, two tables, and two movies and can be found with this article online at doi:10.1016/j.cell.2010.05.003.

ACKNOWLEDGMENTS

We thank Janet Newman at the Bio21 C3 crystallization facility, Clemens Schulze-Briese, support staff at the Swiss Light Source, support staff at the Australian Synchrotron, Marc Kvansakul and Peter Czabotar for help with data collection, Peter Colman, Pauline Crewther, and James Blake for input on the manuscript, and Declan Doyle for the KirBac3.1 construct. We acknowledge assistance from the Australian Synchrotron Research Program for travel to the Swiss Light Source, the Australian National Health and Medical Research Council (NHMRC) for project funding, NHMRC Independent Research Institutes Infrastructure Support Scheme grant number 361646, and Victorian State Government Operational Infrastructure Support grants. J.M.G. thanks the Wellcome Trust for an International Senior Research Fellowship and the Australian Research Council Centre of Excellence in Coherent X-ray Science for travel assistance. O.B.C. is supported by an Australian Postgraduate Award.

Received: November 13, 2009
Revised: February 19, 2010
Accepted: May 5, 2010
Published online: June 3, 2010

REFERENCES

Adams, P.D., Grosse-Kunstleve, R.W., Hung, L.W., Ioerger, T.R., McCoy, A.J., Moriarty, N.W., Read, R.J., Sacchettini, J.C., Sauter, N.K., and Terwilliger, T.C. (2002). PHENIX: building new software for automated crystallographic structure determination. Acta Crystallogr. D Biol. Crystallogr. *D58*, 1948–1954.

Ader, C., Schneider, R., Hornig, S., Velisetty, P., Vardanyan, V., Giller, K., Ohmert, I., Becker, S., Pongs, O., and Baldus, M. (2009). Coupling of activation and inactivation gate in a K+-channel: potassium and ligand sensitivity. EMBO J. *28*, 2825–2834.

Armstrong, C.M. (1969). Inactivation of the potassium conductance and related phenomena caused by quaternary ammonium ion injection in squid axons. J. Gen. Physiol. *54*, 553–575.

Armstrong, C.M. (1971). Interaction of tetraethylammonium ion derivatives with the potassium channels of giant axons. J. Gen. Physiol. *58*, 413–437.

Armstrong, C.M., and Hille, B. (1972). The inner quaternary ammonium ion receptor in potassium channels of the node of Ranvier. J. Gen. Physiol. *59*, 388–400.

Armstrong, N., Jasti, J., Beich-Frandsen, M., and Gouaux, E. (2006). Measurement of conformational changes accompanying desensitization in an ionotropic glutamate receptor. Cell *127*, 85–97.

Ashcroft, F.M., Ashcroft, S.J., and Harrison, D.E. (1988). Properties of single potassium channels modulated by glucose in rat pancreatic beta-cells. J. Physiol. *400*, 501–527.

Battle, A.R., Petrov, E., Pal, P., and Martinac, B. (2009). Rapid and improved reconstitution of bacterial mechanosensitive ion channel proteins MscS and MscL into liposomes using a modified sucrose method. FEBS Lett. *583*, 407–412.

Baukrowitz, T., and Yellen, G. (1995). Modulation of K+ current by frequency and external [K+]: a tale of two inactivation mechanisms. Neuron *15*, 951–960.

Baukrowitz, T., and Yellen, G. (1996). Use-dependent blockers and exit rate of the last ion from the multi-ion pore of a K+ channel. Science *271*, 653–656.

Baukrowitz, T., Tucker, S.J., Schulte, U., Benndorf, K., Ruppersberg, J.P., and Fakler, B. (1999). Inward rectification in KATP channels: a pH switch in the pore. EMBO J. *18*, 847–853.

Bernèche, S., and Roux, B. (2001). Energetics of ion conduction through the K+ channel. Nature *414*, 73–77.

Blunck, R., Cordero-Morales, J.F., Cuello, L.G., Perozo, E., and Bezanilla, F. (2006). Detection of the opening of the bundle crossing in KcsA with fluorescence lifetime spectroscopy reveals the existence of two gates for ion conduction. J. Gen. Physiol. *128*, 569–581.

Cheng, W., Enkvetchakul, D., and Nichols, C. (2009). KirBac1.1: it's an inward rectifying potassium channel. J. Gen. Physiol. *133*, 295–305.

Cordero-Morales, J.F., Cuello, L.G., Zhao, Y., Jogini, V., Cortes, D.M., Roux, B., and Perozo, E. (2006). Molecular determinants of gating at the potassium-channel selectivity filter. Nat. Struct. Mol. Biol. *13*, 311–318.

Cordero-Morales, J.F., Jogini, V., Lewis, A., Vásquez, V., Cortes, D.M., Roux, B., and Perozo, E. (2007). Molecular driving forces determining potassium channel slow inactivation. Nat. Struct. Mol. Biol. *14*, 1062–1069.

Decher, N., Renigunta, V., Zuzarte, M., Soom, M., Heinemann, S.H., Timothy, K.W., Keating, M.T., Daut, J., Sanguinetti, M.C., and Splawski, I. (2007). Impaired interaction between the slide helix and the C-terminus of Kir2.1: a novel mechanism of Andersen syndrome. Cardiovasc. Res. *75*, 748–757.

Doyle, D.A., Morais Cabral, J., Pfuetzner, R.A., Kuo, A., Gulbis, J.M., Cohen, S.L., Chait, B.T., and MacKinnon, R. (1998). The structure of the potassium channel: molecular basis of K+ conduction and selectivity. Science *280*, 69–77.

Gao, L., Mi, X., Paajanen, V., Wang, K., and Fan, Z. (2005). Activation-coupled inactivation in the bacterial potassium channel KcsA. Proc. Natl. Acad. Sci. USA *102*, 17630–17635.

Gazzarrini, S., Kang, M., Abenavoli, A., Romani, G., Olivari, C., Gaslini, D., Ferrara, G., van Etten, J.L., Kreim, M., Kast, S.M., et al. (2009). Chlorella virus ATCV-1 encodes a functional potassium channel of 82 amino acids. Biochem. J. *420*, 295–303.

Gribble, F.M., Tucker, S.J., Seino, S., and Ashcroft, F.M. (1998). Tissue specificity of sulfonylureas: studies on cloned cardiac and beta-cell K(ATP) channels. Diabetes *47*, 1412–1418.

Guo, D., Ramu, Y., Klem, A.M., and Lu, Z. (2003). Mechanism of rectification in inward-rectifier K+ channels. J. Gen. Physiol. *121*, 261–275.

Hardman, R.M., Stansfeld, P.J., Dalibalta, S., Sutcliffe, M.J., and Mitcheson, J.S. (2007). Activation gating of hERG potassium channels: S6 glycines are not required as gating hinges. J. Biol. Chem. *282*, 31972–31981.

Hille, B. (1992). Ionic Channels of Excitable Membranes, Second Edition (Sunderland, MA: Sinauer Associates Inc.).

Hoshi, T., Zagotta, W.N., and Aldrich, R.W. (1991). Two types of inactivation in Shaker K+ channels: effects of alterations in the carboxy-terminal region. Neuron *7*, 547–556.

Huang, C.L., Feng, S., and Hilgemann, D.W. (1998). Direct activation of inward rectifier potassium channels by PIP2 and its stabilization by Gbetagamma. Nature *391*, 803–806.

Jiang, Y., Lee, A., Chen, J., Cadene, M., Chait, B.T., and MacKinnon, R. (2002). Crystal structure and mechanism of a calcium-gated potassium channel. Nature *417*, 515–522.

Jones, P.A., Tucker, S.J., and Ashcroft, F.M. (2001). Multiple sites of interaction between the intracellular domains of an inwardly rectifying potassium channel, Kir6.2. FEBS Lett. *508*, 85–89.

Kollewe, A., Lau, A.Y., Sullivan, A., Benoît Roux, and Goldstein, S.A. (2009). A structural model for K2P potassium channels based on 23 pairs of interacting sites and continuum electrostatics. J. Gen. Physiol. *134*, 53–68.

Kraulis, P. (1991). MOLSCRIPT: A program to produce both detailed and schematic plots of protein structures. J. Appl. Crystallogr. *24*, 946–950.

Kubo, Y., and Murata, Y. (2001). Control of rectification and permeation by two distinct sites after the second transmembrane region in Kir2.1 K+ channel. J. Physiol. *531*, 645–660.

Kuo, A., Gulbis, J.M., Antcliff, J.F., Rahman, T., Lowe, E.D., Zimmer, J., Cuthbertson, J., Ashcroft, F.M., Ezaki, T., and Doyle, D.A. (2003). Crystal structure of the potassium channel KirBac1.1 in the closed state. Science *300*, 1922–1926.

Logothetis, D.E., Jin, T., Lupyan, D., and Rosenhouse-Dantsker, A. (2007). Phosphoinositide-mediated gating of inwardly rectifying K(+) channels. Pflugers Arch. *455*, 83–95.

Lopatin, A.N., Makhina, E.N., and Nichols, C.G. (1994). Potassium channel block by cytoplasmic polyamines as the mechanism of intrinsic rectification. Nature *372*, 366–369.

Lopes, C.M., Zhang, H., Rohacs, T., Jin, T., Yang, J., and Logothetis, D.E. (2002). Alterations in conserved Kir channel-PIP2 interactions underlie channelopathies. Neuron *34*, 933–944.

Loussouarn, G., Marton, L.J., and Nichols, C.G. (2005). Molecular basis of inward rectification: structural features of the blocker defined by extended polyamine analogs. Mol. Pharmacol. *68*, 298–304.

Lu, T., Ting, A.Y., Mainland, J., Jan, L.Y., Schultz, P.G., and Yang, J. (2001). Probing ion permeation and gating in a K+ channel with backbone mutations in the selectivity filter. Nat. Neurosci. *4*, 239–246.

Matsuda, H., Saigusa, A., and Irisawa, H. (1987). Ohmic conductance through the inwardly rectifying K channel and blocking by internal Mg2+. Nature *325*, 156–159.

Miller, C. (1987). Trapping single ions inside single ion channels. Biophys. J. *52*, 123–126.

Osawa, M., Yokogawa, M., Muramatsu, T., Kimura, T., Mase, Y., and Shimada, I. (2009). Evidence for the direct interaction of spermine with the inwardly rectifying potassium channel. J. Biol. Chem. *284*, 26117–26126.

Riven, I., Kalmanzon, E., Segev, L., and Reuveny, E. (2003). Conformational rearrangements associated with the gating of the G protein-coupled potassium channel revealed by FRET microscopy. Neuron *38*, 225–235.

Shang, L., and Tucker, S.J. (2008). Non-equivalent role of TM2 gating hinges in heteromeric Kir4.1/Kir5.1 potassium channels. Eur. Biophys. J. *37*, 165–171.

Shin, H.G., Xu, Y., and Lu, Z. (2005). Evidence for sequential ion-binding loci along the inner pore of the IRK1 inward-rectifier K+ channel. J. Gen. Physiol. *126*, 123–135.

Sobolevsky, A.I., Rosconi, M.P., and Gouaux, E. (2009). X-ray structure, symmetry and mechanism of an AMPA-subtype glutamate receptor. Nature *462*, 745–756.

Soom, M., Schönherr, R., Kubo, Y., Kirsch, C., Klinger, R., and Heinemann, S.H. (2001). Multiple PIP2 binding sites in Kir2.1 inwardly rectifying potassium channels. FEBS Lett. *490*, 49–53.

Strong, M., Sawaya, M.R., Wang, S., Phillips, M., Cascio, D., and Eisenberg, D. (2006). Toward the structural genomics of complexes: crystal structure of a PE/PPE protein complex from Mycobacterium tuberculosis. Proc. Natl. Acad. Sci. USA *103*, 8060–8065.

Taglialatela, M., Ficker, E., Wible, B.A., and Brown, A.M. (1995). C-terminus determinants for Mg2+ and polyamine block of the inward rectifier K+ channel IRK1. EMBO J. *14*, 5532–5541.

Tao, X., Avalos, J.L., Chen, J., and MacKinnon, R. (2009). Crystal structure of the eukaryotic strong inward-rectifier K+ channel Kir2.2 at 3.1 A resolution. Science *326*, 1668–1674.

Thompson, A.N., Kim, I., Panosian, T.D., Iverson, T.M., Allen, T.W., and Nimigean, C.M. (2009). Mechanism of potassium-channel selectivity revealed by Na(+) and Li(+) binding sites within the KcsA pore. Nat. Struct. Mol. Biol. *16*, 1317–1324.

Tucker, S.J., Gribble, F.M., Proks, P., Trapp, S., Ryder, T.J., Haug, T., Reimann, F., and Ashcroft, F.M. (1998). Molecular determinants of KATP channel inhibition by ATP. EMBO J. *17*, 3290–3296.

Vandenberg, C.A. (1987). Inward rectification of a potassium channel in cardiac ventricular cells depends on internal magnesium ions. Proc. Natl. Acad. Sci. USA *84*, 2560–2564.

Wible, B.A., Taglialatela, M., Ficker, E., and Brown, A.M. (1994). Gating of inwardly rectifying K+ channels localized to a single negatively charged residue. Nature *371*, 246–249.

Wilkens, C.M., and Aldrich, R.W. (2006). State-independent block of BK channels by an intracellular quaternary ammonium. J. Gen. Physiol. *128*, 347–364.

Yang, J., Jan, Y.N., and Jan, L.Y. (1995). Control of rectification and permeation by residues in two distinct domains in an inward rectifier K+ channel. Neuron *14*, 1047–1054.

Yellen, G., Jurman, M.E., Abramson, T., and MacKinnon, R. (1991). Mutations affecting internal TEA blockade identify the probable pore-forming region of a K+ channel. Science *251*, 939–942.

Yohannan, S., Hu, Y., and Zhou, Y. (2007). Crystallographic study of the tetrabutylammonium block to the KcsA K+ channel. J. Mol. Biol. *366*, 806–814.

Zhou, Y., Morais-Cabral, J.H., Kaufman, A., and MacKinnon, R. (2001). Chemistry of ion coordination and hydration revealed by a K+ channel-Fab complex at 2.0 A resolution. Nature *414*, 43–48.